Materials Research Proceedings 57 (2025) 242-249 https://doi.org/10.21741/9781644903735-28

Experimental characterization of QP1180 steel and its performance in stamping simulation: Comparison with DP1180

Maria Emanuela Palmieri[1,*], Matteo Villa[1], Michele Abruzzo[2], Giuseppe Macoretta[2], Stefania Bruschi[3] and Luigi Tricarico[1]

[1]Department of Mechanical, Mathematic and Management, Polytechnic of Bari, Bari, 70125, Italy

[2]Department of Civil and Industrial Engineering, University of Pisa, Pisa, Italy

[3]Deptartment of Industrial Engineering, University of Padova, Padova, Italy

[*]mariaemanuela.palmieri@poliba.it

Keywords: Stamping, High Strength Steel, Deformation-Induced Martensitic Transformation

Abstract. The increasing demand for lighter vehicles and improved safety has driven the adoption of Advanced High-Strength Steels (AHSS). Among these, third-generation Quenching and Partitioning (QP) steels stand out for their exceptional combination of ultra-high strength and ductility, attributed to the TRansformation-Induced Plasticity (TRIP) effect, making them highly suitable for automotive applications. This study focuses on the characterization of QP1180 steel using tensile tests, complemented by Digital Image Correlation (DIC) to analyze mechanical behavior in different rolling directions (0°, 90°, 45°). The data obtained were then integrated into Finite Element (FE) software to simulate the stamping process of a B-Pillar. The simulation results were compared with those obtained from simulating the stamping process of a first-generation steel, DP1180, with a similar tensile strength. Finally, fractographic and microstructural analyses were performed to deepen the understanding of the steel's fracture mechanisms.

Introduction

The automotive industry today is increasingly focused on refining materials to improve vehicle performance, especially in terms of reducing weight, saving energy, and enhancing corrosion resistance. In this context, Advanced High-Strength Steels (AHSS) have become crucial [1-2]. Among them, Dual-Phase (DP) steel, part of the first generation of AHSS, is extensively used due to its combination of high work-hardening, high strength, and good ductility [1, 3]. Its microstructure, which consists of a softer ferrite phase combined with a harder martensite phase through intercritical annealing, results in a material with strength ranging from 500 to 1000 MPa and strain from 5% to 20% [4-7].

Recently, there has been growing interest in third-generation AHSS, such as Quenching and Partitioning (QP) steels, which offer mechanical strength between 600 and 1200 MPa and significantly greater plastic strain at fracture (15% to 30%) compared to DP steels. This enhanced deformability derives from multiphase hardening coupled with Transformation-Induced Plasticity (TRIP), due to the presence of metastable Retained Austenite (RA) [8–10]. QP steels are typically produced by austenitizing above the Ac_3 temperature, followed by rapid cooling between the martensite start (M_s) and finish (M_f) temperatures, and then a partitioning treatment to promote C diffusion from martensite to austenite [11]. This process results in a triphasic microstructure of C-rich martensite, C-poor tempered martensite (essentially ferrite), and RA, leveraging DIMT to improve toughness. Understanding and controlling this transformation is essential for optimizing performance and predicting material behavior. While AHSS properties are typically assessed through quasi-static uniaxial tensile tests at room temperature, it is evident that DIMT is also

Content from this work may be used under the terms of the Creative Commons Attribution 3.0 license. Any further distribution of this work must maintain attribution to the author(s) and the title of the work, journal citation and DOI. Published under license by Materials Research Forum LLC.

Materials Research Proceedings 57 (2025) 242-249 https://doi.org/10.21741/9781644903735-28

influenced by strain rate, temperature evolution during testing, and RA grain orientation—which is affected by sheet orientation (i.e., rolling vs test direction) [12-13]. These factors can be leveraged to control the martensitic transformation in QP steels during stamping processes. Understanding these influences will enable process optimization, fine-tuning forming responses and tailoring the stamped components' properties. This study will focus on investigating the mechanical properties of QP1180 steel in relation to sheet orientation. By analyzing fracture surfaces and the microstructure of broken specimens, we aim to establish a correlation between sheet orientation and fracture mechanisms. Furthermore, since accurately predicting the plastic behavior of textured sheet metals is crucial for reliable numerical analysis of sheet deformation, the mechanical characterization data will be integrated into a Finite Element (FE) simulation software to model the stamping process of an automotive structural component—the B-Pillar. Finally, QP1180 will be compared to the first-generation DP1180 steel to assess mechanical performance, formability, and determine which material can be used to produce the highest-quality component at the end of the stamping process. The novelty of this study lies in its comprehensive mechanical and numerical investigation of the underexplored QP1180 steel, moving beyond prior research that mainly addresses microstructural evolution or basic tensile behavior. By integrating mechanical characterization with realistic forming simulations of an automotive component, this work provides original data on the material's anisotropic response and delivers valuable insights to support its industrial application.

Materials and Method

In this study, QP1180 steel—a third-generation AHSS of interest for automotive stamping of structural components—was analyzed. Commercial 1.2 mm thick QP1180 sheets were supplied by Centro Ricerche FIAT (CRF) – Stellantis in the quenched and partitioned condition with zinc coated surfaces.

The first phase involved mechanical characterization at room temperature through uniaxial tensile tests on specimens oriented at various angles relative to the Rolling Direction (RD) to understand the material's anisotropic behavior. The experimental data (flow curve, Young's modulus, and anisotropy coefficients) were used for the numerical simulation of an automotive B-Pillar stamping process (Fig. 1 (a)).

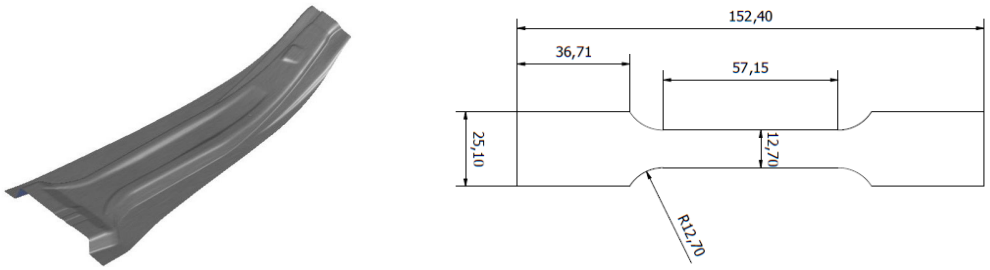


Fig. 1: Geometry of B-Pillar (a) and specimen for tensile testing with dimensions in mm (b)

The tensile tests were performed using an Instron 4485 universal testing machine, electronically controlled by the Zwick-Roell software, with a crosshead speed set to 1 mm/min. Strain measurements were conducted using the digital image correlation system (DIC - Aramis, provided by GOM), enabling a detailed analysis of the strain field. Specifically, the strain along the loading direction ($\varepsilon_{(0°/90°/45°),L}$) was determined using a video extensometer with a gauge length of 30 mm, while the strain along the transverse direction ($\varepsilon_{(0°/90°/45°),w}$) was measured with a video extensometer with a 9 mm gauge length. The anisotropy coefficients were calculated according to Eq. 1.

Materials Research Proceedings 57 (2025) 242-249 https://doi.org/10.21741/9781644903735-28

$$r_{0°/90°/45°} = \frac{\varepsilon_{(0°/90°/45°),w}}{-(\varepsilon_{(0°/90°/45°),L}+\varepsilon_{(0°/90°/45°),w})} \quad (1)$$

While this method does not fully comply with ISO 10113 standard, recent studies [14] support the use of DIC for preliminary anisotropy evaluation.

Fig. 1 (b) shows the geometry of the tensile test specimens; three specimens per direction were tested to ensure reliable results.

Metallographic investigations were performed on samples taken both parallel and perpendicular to the sheet plane, with the latter showing a surface orthogonal to the RD. Samples were ground with 1200 SiC paper, polished with diamond suspension, and etched with Nital.

Fractographic analyses examined the fracture surfaces to assess the influence of orientation relative to the RD. Scanning electron microscopy was carried out using a FEI QUANTA 450 ESEM-FEG at CISUP, University of Pisa.

The stamping process was simulated with AutoForm®R10. The blank was defined at 1.2 mm thickness (matching the test specimens), and the tooling geometries were modeled as shown in Fig. 2 (a). A forming speed of 295 mm/s was used with uniform lubrication (1 g/m²). Frictional behavior was modeled using a variable friction law generated in TriboForm®, based on lubrication quantity and contact conditions, with an average friction coefficient of 0.099. The punch and die were considered rigid tools, while the blank holder was controlled using a force-based approach, with a value set at 1000 kN, determined through preliminary simulations aimed at optimizing component quality by minimizing wrinkling and preventing splits.

To evaluate the effect of mechanical properties, the simulation was repeated using DP1180 steel, with material data from Baosteel (no experimental tests were performed). For an accurate numerical simulation of the stamping process and a reliable assessment of the final component's quality, it is essential to integrate the Formability Limit Curve (FLC) into the FE software. Although future studies are planned to derive it for QP1180 steel, this work has opted to use the curve provided by Baosteel. Fig. 2 (b) presents the forming limit curves for both QP1180 and DP1180 steels.

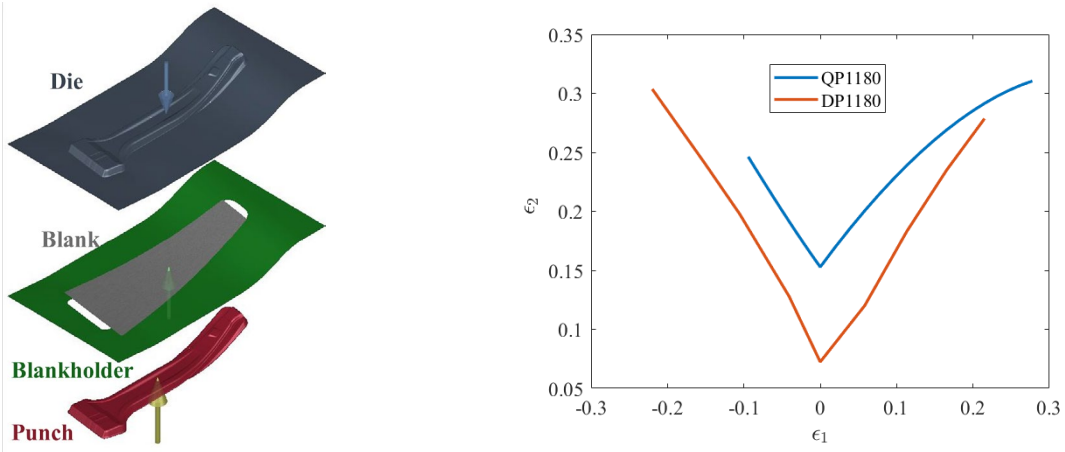


Fig. 2: Tool geometry (a) and formability limit curves for QP1180 steel and DP1180 steel provided by Baosteel (b)

As detailed in the results, differences in the mechanical properties of the two materials affect process performance, enhancing the understanding of high-strength steels in industrial applications.

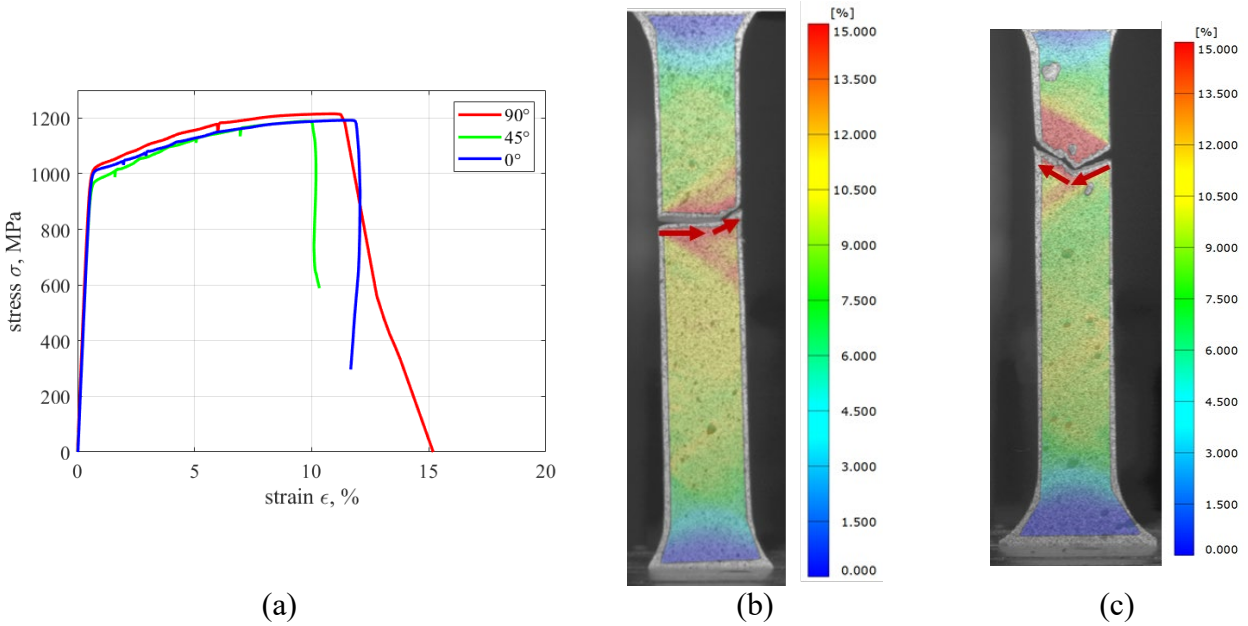
Materials Research Proceedings 57 (2025) 242-249 https://doi.org/10.21741/9781644903735-28

Tensile testing results

The tensile test results, shown as engineering stress-strain curves in Fig. 3a, are compared for the three RDs. The average curve from three tests is presented for each specimen orientation relative to the sheet RD.

The comparison reveals minimal anisotropic strength under uniaxial tension. Specimens cut at 90° to the RD show the highest strength, while those at 45° exhibit the lowest strength and elongation at fracture. These findings align with the literature [15].

Thanks to the use of the DIC technique, it was possible to perform a detailed analysis of the fracture mode and the strain distribution occurring during the tensile test. This methodology allowed for precise information on the localization of strains in the sample and their evolution up to the moment of fracture.



(a) (b) (c)

Fig. 3: (a) Average engineering stress-strain curves for different specimen orientations and DIC strain maps at fracture for specimens cut along the RD (b) and at 45° (c)

Figures 3b and 3c compares strain maps at fracture onset for two specimen types: one cut along the RD (Fig. 3 (b)) and another at a 45° angle (Fig. 3 (c)). Specimens cut at 90° to the RD showed a fracture mode similar to those cut along the RD, indicating comparable mechanical behavior.

The fracture initiation and propagation mechanisms, highlighted by arrows in the figures, show that in RD-oriented specimens, cracks start at the edge, propagate transversely, then deviate at an angle, leading to complete failure. In specimens cut at 45° to the RD, cracks initiate at the edge, propagate at an inclined angle, and form a V-shaped fracture upon reaching the center.

Table 1: Anisotropy values and yield stress ratios for definition of yield surface according to BBC 2005 model.

r_0	0.681
r_{45}	0.776
r_{90}	0.701
σ_0/σ_0	1
σ_{45}/σ_0	0.972
σ_{90}/σ_0	1.019

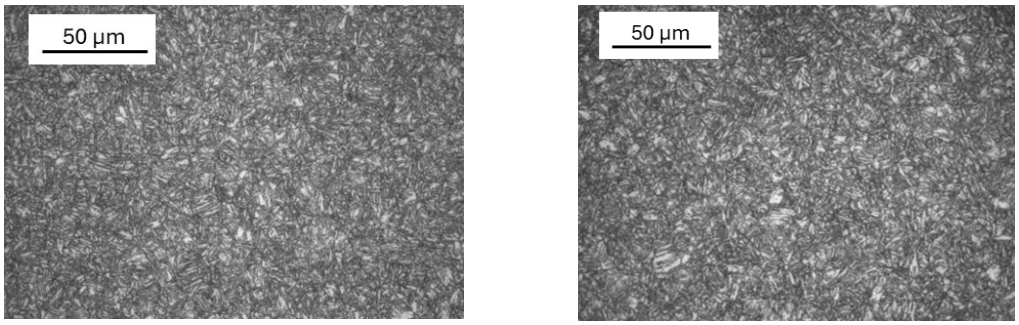
The elastic modulus was determined to be 200 ± 2.1 GPa. The true flow curve was derived from the engineering stress-strain curves and input into FE software. To define the yield surface, the

Materials Research Proceedings 57 (2025) 242-249 https://doi.org/10.21741/9781644903735-28

BBC 2005 model [16] was used, with input parameters including the anisotropy coefficients (r_0, r_{45}, r_{90}) and yield stress ratios, as shown in Table 1.

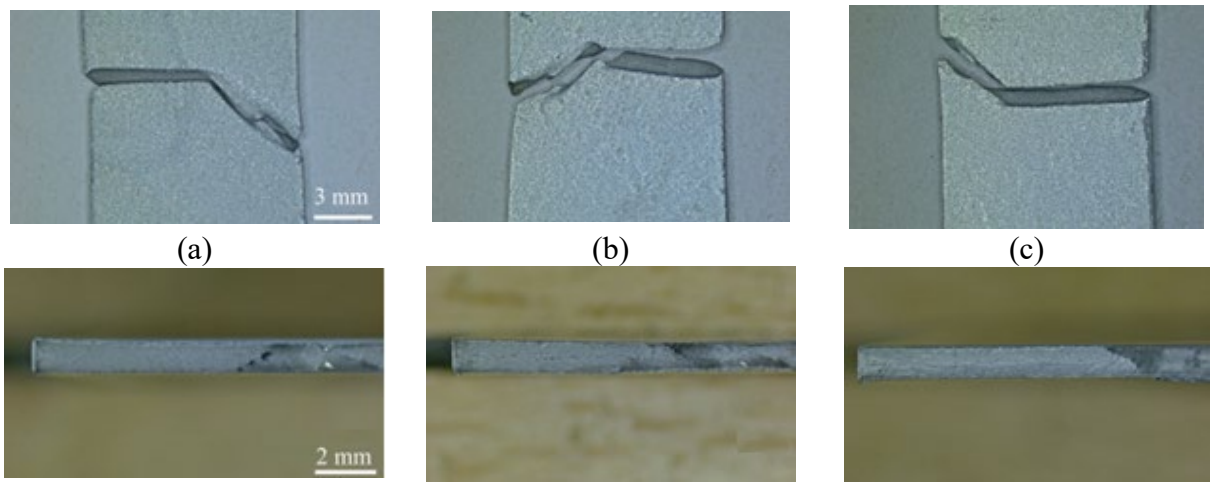
Fractographic and microstructural observations

The as-received material's microstructure consists of a fine martensitic matrix with ferritic islands and occasional RA regions, as shown in Fig. 4. The RD did not affect the microstructure, as the final QP heat treatment produced an isotropic martensitic matrix. This microstructure aligns with recent literature on the as-received material [17].



(a) (b)

Fig. 4: Microstructure of as-received material, samples extracted in direction (a) perpendicular and (b) parallel to the sheet plane.



(a) (b) (c)

(d) (e) (f)

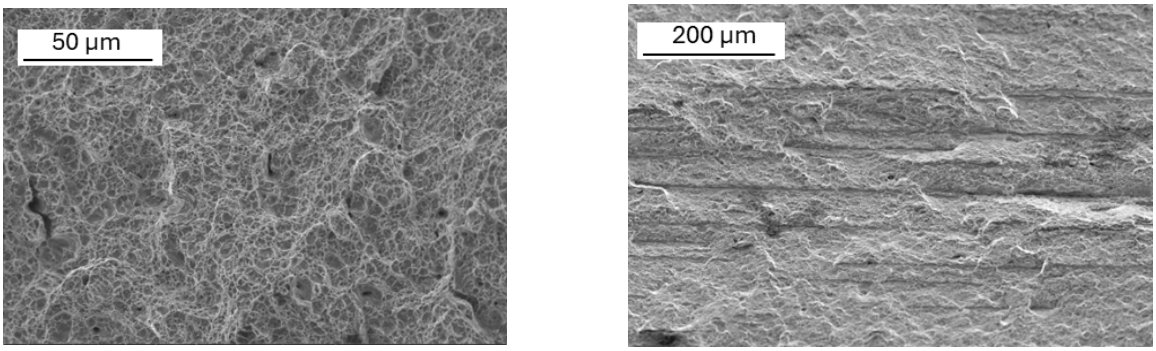
Fig. 5: Fracture surfaces of the tensile specimens observed via stereomicroscope. Specimens extracted at 0°(a) (d), 45°(b) (e), and 90° (c) (f) to the sheet RD

The fracture surface of the tensile specimens featured a wide region of ductile fracture, irrespectively on the angle between the specimen longitudinal axis and the sheet RD. As previously observed from DIC monitoring, the fracture surface presented a wide portion orthogonal to the loading direction and an small region angled at about 45° in proximity to the specimen edges for both the 0° and 90° specimens, Fig. 5. The specimen extracted at 45° to the RD, presented instead two angled surfaces. No macroscopic defects were observed for all the specimens.

As shown in Fig. 6, SEM investigations confirmed the ductile nature of the fracture surface, characterized by the presence of dimples having a dimension consistent with the elongation at fracture in line with the results of the tensile tests. For the samples extracted at 45° and 90° to the sheet RD, the SEM investigation revealed the presence of elongated segregation bands in the middle of the sheet thickness. Those bands, which were not evident from metallographic

Materials Research Proceedings 57 (2025) 242-249 https://doi.org/10.21741/9781644903735-28

investigations, could be produced by the combined effect of the structure produced by the sheet rolling and the TRIP effect occurring during the tensile test.



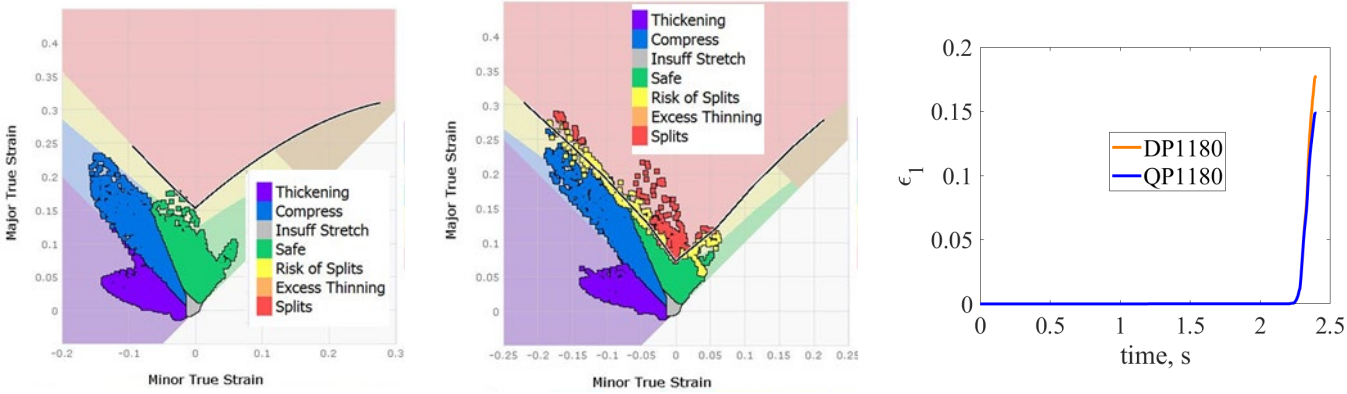
(a) (b)

Fig. 6: Fracture surfaces observed via SEM. Ductile fracture dimples observed for all the specimens(a), segregation bands from a specimen at 90° to the sheet RD (b).

Although not directly used in the FE model, fractographic and microstructural analyses support the modeling assumptions by confirming the ductile fracture behavior and the absence of critical defects, in line with the FLC-based approach.

FE results

The numerical simulation of the B-Pillar stamping process assessed the deformational behavior of DP1180 and QP1180 under identical conditions, using the Forming Limit Diagram (FLD) to evaluate failure susceptibility. The results revealed distinct formability responses. The QP1180 component showed favorable behavior, with principal stresses staying below the forming limit curve in all areas (Fig. 7 (a)), reflecting its superior mechanical properties, higher ductility, and better plastic deformation absorption. In contrast, the DP1180 component showed criticalities, with stresses exceeding the forming limit curve in areas of high deformation, such as curvature radii and stretching zones, leading to fractures (Fig. 7 (b)).The difference in material response is due to their distinct microstructures. QP1180, with its multiphase microstructure and metastable RA, offers superior strength and ductility compared to the older DP1180, a dual-phase steel with a ferrite-martensite structure that provides high strength but lower ductility and plastic deformation capacity.



(a) (b) (c)

Fig. 7: Formability results for (a) QP1180 (b) DP1180; and (c) comparison of the major strain over time at the critical point of the component for the two steels.

To complement the FLD-based evaluation and enable a more objective comparison, the major strain was mapped on the stamped components for both steels. The strain maps reveal that DP1180

exhibits higher major strain in critical areas (curvature and flange), indicating a greater ability to undergo plastic deformation before localization. In contrast, QP1180 shows lower major strain values overall, despite its superior mechanical strength, suggesting more localized deformation due to its higher yield strength and rigid martensitic matrix. This may delay necking in moderate strain zones but increase the risk of sudden failure if strain localization occurs. Figure 7c shows the time evolution of major strain in a critical area for both steels. This behavior also affects thickness reduction: DP1180 shows more pronounced, evenly distributed thinning, while QP1180 exhibits less thinning but more localized reductions in critical areas.

Conclusions

The mechanical behavior and formability of QP1180 steel were studied through experiments and simulations, compared to DP1180 steel. Key findings include:

- Tensile tests showed slight anisotropy in QP1180, with the highest strength in specimens cut at 90° to the RD and the lowest at 45°. The QP heat treatment results in an isotropic martensitic matrix.
- DIC analysis allowed for detailed observation of strain distribution and localization. Moreover, the image sequence acquired by the DIC system enabled the identification of fracture propagation patterns. Specimens at 0° and 90° showed a combination of transverse and oblique crack paths, while 45° specimens exhibited a characteristic V-shaped fracture. SEM analysis confirmed the ductile nature of the failure.
- Numerical simulation of the B-Pillar stamping process showed QP1180's superior formability due to its multiphase microstructure and metastable RA, which enhance ductility and plastic deformation.

These findings demonstrate the potential of QP1180 for high-strength, ductile automotive structural components.

Acknowledgments

Financed by the European Union - NextGenerationEU (National Sustainable Mobility Center CN00000023, Italian Ministry of University and Research Decree n. 1033 - 17/06/2022, Spoke 11 - Innovative Materials & Lightweighting). The authors are also grateful to AutoForm Engineering GmbH for the support in FE model and MANAGE 5.0 project (F/310302/01-05/X56) for its contribution to the research activities.

References

[1] J. Huang, S. Li, H. Zhong, S. Xiao, D. Li, Microstructure, mechanical properties, and corrosion behavior of laser-welded dissimilar joints between DP980 and QP980 steel, Steel Res. Int. 93 (2022) 2100541. https://doi.org/10.1002/srin.202100541

[2] D.K. Matlock, S. Kang, E. De Moor, J.G. Speer, Applications of rapid thermal processing to advanced high strength sheet steel developments, Mater. Charact. 166 (2020) 110397. https://doi.org/10.1016/j.matchar.2020.110397

[3] F. Badkoobeh, A. Nouri, H. Hassannejad, H. Mostaan, Microstructure and mechanical properties of resistance spot welded dual-phase steels with various silicon contents, Mater. Sci. Eng. A 790 (2020) 139703. https://doi.org/10.1016/j.msea.2020.139703

[4] D.K. Kim, H.J. Kim, S. Gong, S.E. Shin, S.J. Lee, A comparative study on the wear behavior of dual phase (DP) steel and quenching and partitioning (QP) steel, Tribol. Int. 194 (2024) 109445. https://doi.org/10.1016/j.triboint.2024.109445

[5] D.K. Kim, H.J. Kim, S. Gong, S.E. Shin, S.J. Lee, A comparative study on the wear behavior of dual phase (DP) steel and quenching and partitioning (QP) steel, Tribol. Int. 194 (2024) 109445. https://doi.org/10.1016/j.triboint.2024.109445

[6] R. Kuziak, R. Kawalla, S. Waengler, Advanced high strength steels for automotive industry, Arch. Civ. Mech. Eng. 8 (2008) 103-117. https://doi.org/10.1016/S1644-9665(12)60197-6

[7] O. Kwon, K.Y. Lee, G.S. Kim, K.G. Chin, New trends in advanced high strength steel developments for automotive application, Mater. Sci. Forum 638 (2010) 136-141. https://doi.org/10.4028/www.scientific.net/MSF.638-642.136

[8] H. Jirková, L. Kučerová, B. Mašek, Effect of quenching and partitioning temperatures in the QP process on the properties of AHSS with various amounts of manganese and silicon, Mater. Sci. Forum 706 (2012) 2734-2739. https://doi.org/10.4028/www.scientific.net/MSF.706-709.2734

[9] Q. Liu, Q. Zhou, J. Venezuela, M. Zhang, A. Atrens, Hydrogen concentration in dual-phase (DP) and quenched and partitioned (Q&P) advanced high-strength steels (AHSS) under simulated service conditions compared with cathodic charging conditions, Adv. Eng. Mater. 18 (2016) 1588-1599. https://doi.org/10.1002/adem.201600217

[10] H.L. Yi, L. Sun, X.C. Xiong, Challenges in the formability of the next generation of automotive steel sheets, Mater. Sci. Technol. 34 (2018) 1112-1117. https://doi.org/10.1080/02670836.2018.1424383

[11] H.J. Kim, M.G. Lee, Analysis of hydrogen trapping behaviour in plastically deformed quenching and partitioning steel in relation to microstructure evolution by phase transformation, J. Alloys Compd. 904 (2022) 164018. https://doi.org/10.1016/j.jallcom.2022.164018

[12] J. Hu, G. Thomas, Evolving the “Banana Chart”: Temperature and strain rate effects on tensile properties of new-generation advanced high-strength steels, JOM 73 (2021) 3204-3213. https://doi.org/10.1007/s11837-021-04900-x

[13] C.B. Finfrock, Temperature and strain rate dependence of the martensitic transformation and mechanical properties in advanced high strength steels, Ph.D. dissertation, Colorado School of Mines, 2022. 10.3389/fmats.2020.615361

[14] E. Seidi, S.F. Miller, F. Kaviari, L. Huang, T.B. Stoughton, Novel method to assess anisotropy in formability using DIC, Int. J. Mech. Sci. 285 (2025) https://doi.org/10.1016/j.ijmecsci.2024.109782

[15] C. Zhang, Y. Wang, Z. Chen, N. Yang, Y. Lou, T. Clausmeyer, Q. Zhang, Characterization of plasticity and fracture of a QP1180 steel sheet, Procedia Manuf. 50 (2020) 529–534. https://doi.org/10.1016/j.promfg.2020.08.095

[16] D. Banabic, Sheet Metal Forming Processes: Constitutive Modelling and Numerical Simulation, Springer Science & Business Media, 2010.

[17] W. Li, W. Wu, Q. Zhou, W. Li, J. Li, Analysis of hydrogen-induced delayed cracking and hydrogen trapping behavior in plastically deformed quenching and partitioning steel, Corros. Sci. 223 (2023) 111437. https://doi.org/10.1016/j.corsci.2023.111437.